J. Assoc. Res. Otolaryngol. 21(1): 21-32 (2020)

A non-linear viscoelastic model of the incudostapedial joint

Majid Soleimani[1], W. Robert J. Funnell[1,2], Willem F. Decraemer[3]

[1]Department of BioMedical Engineering, McGill University, Montréal, Canada

[2]Department of Otolaryngology – Head and Neck Surgery, McGill University, Montréal, Canada

[3]Department of Biomedical Physics,University of Antwerp, Antwerpen, Belgium

Correspondence to robert.funnell@mcgill.ca

Abstract

The ossicular joints of the middle ear can significantly affect middle-ear function, particularly under conditions such as high-intensity sound pressures or high quasi-static pressures. Experimental investigations of the mechanical behaviour of the human incudostapedial joint have shown strong non-linearity and asymmetry in tension and compression tests, but some previous finite-element models of the joint have had difficulty replicating such behaviour. In this paper, we present a finite-element model of the joint that can match the asymmetry and non-linearity well without using different model structures or parameters in tension and compression. The model includes some of the detailed structures of the joint seen in histological sections. The material properties are found from the literature when available, but some parameters are calculated by fitting the model to experimental data from tension, compression and relaxation tests. The model can predict the hysteresis loops of loading and unloading curves. A sensitivity analysis for various parameters shows that the geometrical parameters have substantial effects on the joint mechanical behaviour. While the joint capsule affects the tension curve more, the cartilage layers affect the compression curve more.

Keywords: middle ear, ossicular chain, incudostapedial joint, finite-element, mechanical behaviour

Introduction

The ossicular chain of the human middle ear includes two joints that connect the three ossicles to one another: the incudomallear and incudostapedial joints. The incudostapedial joint (ISJ), the smallest joint in the human body (e.g., Karmody et al., 2009), lies between the lenticular plate of the incus (LPI) and the stapes head (SH). As a synovial joint, it consists of articular cartilage layers that are separated by a synovial gap filled with synovial fluid (SF). A ligamentous joint capsule encloses the joint structure.

For normal sound pressures, the middle ear is usually considered to function as a linear impedance

transformer that improves the energy transfer from the low-acoustical-impedance air in the external ear to the high-acoustical-impedance liquid in the cochlea. However, the flexibility of the ossicular joints may contribute to additional roles for the middle ear under some conditions. Non-linear actions of the ossicular joints have been suggested (e.g., Price & Kalb, 1991; Cheng et al., 2017). Even in the linear case, Gottlieb et al. (2018) showed, by fixing each of the ossicular joints separately, that the joints can reduce the peak amplitude (and increase the width) of potentially damaging impulsive stimuli, which may protect the hair cells in the cochlea. The early middle-ear model of Zwislocki (1957) had already suggested the filtering effect of the incudostapedial joint. Moreover, the contributions of the joints to the middle-ear response at the high quasi-static pressures that occur during tympanometry, for example, have yet to be considered (Qi et al. 2008). These observations motivate further study on the mechanical behaviour of the ossicular joints.

A few experimental and numerical investigations have been conducted on the mechanical behaviour of the ISJ. Ghosh and Funnell (1995) performed an early exploration of the effects of ISJ flexibility in a very simple finite-element (FE) model of the cat middle ear. Funnell et al. (2005, 2006) numerically investigated the function of the ISJ in cat and human with a FE model to compare the flexibility of the incudal pedicle and the ISJ. For moderate sound pressures, FE modelling of the joints as blocks of visco-elastic material has been shown to result in satisfactory agreement with experimental data, particularly at low frequencies (Maftoon et al. 2015; O'Connor et al. 2017). However, for higher pressures and frequencies it may be necessary to use detailed models of the joints (Gottlieb et al. 2018). To obtain experimental data relevant to large quasi-static pressures, Gea (2010) recorded X-ray microCT scans of intact human and gerbil middle ears while the tympanic membrane was under static pressures. He determined the distance between the LPI and SH as a function of the applied pressure. Zhang and Gan (2011) extracted incus-stapes samples from fresh human temporal bones; performed

tension, compression, relaxation and failure tests; and then compared the experimental results with a FE model that included several components of the ISJ. The model was later incorporated into a middle-ear model (Gan and Wang 2015). Recently the same group used a dynamic mechanical analyzer and frequency-temperature superposition to measure the dynamic mechanical properties of the ISJ over a wide frequency range, and again fitted a FE model to the data (Jiang and Gan 2018). Both Gea (2010) and Zhang and Gan (2011) observed a strong non-linearity in their experiments on the quasi-static mechanical response of the ISJ, and a strong asymmetry between tension and compression.

Decraemer et al. (2015) developed several FE models of human and gerbil ISJs, including their various components, and tried to reproduce the non-linearity and strong asymmetry observed in experimental quasi-static tension and compression tests. In Soleimani and Funnell (2016, 2018), we simplistically modelled the joint capsule with a membrane, analytically studied the mechanical behaviour of the joint, and concluded that the nonlinear asymmetric behaviour may be due to a mechanical instability of the joint capsule that is governed mainly by the joint-capsule length and the amount of SF in the joint. We subsequently presented a more realistic FE model of the human ISJ (Soleimani et al. 2018) and investigated the sensitivity of the model to several geometrical and mechanical properties to determine potential sources for the asymmetric and nonlinear behaviour of the joint. However, as discussed below, these and earlier numerical models either failed to fit the experimental data or included physiologically unrealistic assumptions.

Several assumptions have been used in the past to produce the desired strong asymmetry in FE models of the ISJ. In the model of Zhang and Gan (2011), “the adhesive force on the contact surface between fluid and cartilage was not taken into account”, thus unrealistically decoupling the normal displacements under tension. It seems that the same assumption was used by Gan and Wang (2015) and Jiang and Gan (2018). In the simulations of an FE model for the gerbil ISJ by Decraemer et al. (2015),

the cartilage layers came into contact during compression. This assumption agrees with those histological sections of the ISJ where a very thin or even undetectable layer of SF is observed within the synovial gap, and with experimental observations by Gea (2010) both for human and gerbil ISJ. However, with this assumption the ISJ of the model became too stiff compared with the experimental data. We also tried to relate the asymmetry to a mechanical instability in the capsule with an analytical approach and a membrane approximation for the capsule (Soleimani and Funnell 2016, 2018), the instability being controlled mainly by capsule length and the volume of the SF. We also implemented that theory in a FE model with a thick capsule (Soleimani et al. 2018) by removing some of the SF from the synovial gap, resulting in an increased asymmetry but without any instability occurring. However, the model with a change in the SF volume was very complicated and difficult to justify.

In this article, we present a new FE model for the human ISJ in which the asymmetry is produced with realistic geometries for the capsule and the cartilage (see figure 1) and with realistic coupling between the SF and the solid structures. We estimated the geometrical parameters (the length and thickness of the joint capsule and the gap between the bony surfaces) from eight histological sections of the human ISJ from five different ears. For some of the material properties we relied on experimental data for synovial joints in other parts of the body, and some of the properties are calculated by fitting our model to the experimental tension, compression and relaxation data of Zhang and Gan (2011) for the human ISJ. Unlike previous FE models, this model does not assume different boundary conditions in tension and compression to model asymmetry and nonlinearity. The new model is used to simulate the hysteresis of the ISJ (i.e., the difference between the loading and unloading curves in the tension and compression tests) for the first time. A sensitivity analysis is performed to determine the most influential geometrical and material properties.

Methods

EXPERIMENTAL DATA

The experiments of Zhang and Gan (2011) were performed on isolated incus-and-stapes samples extracted from fresh human temporal bones. The incus long process was connected to an isometric load cell, and the stapes was displaced perpendicular to the footplate. A pre-load of 0.001 N was applied to set the initial joint configuration. For the tension and compression tests, the joints were elongated by 0.2 mm and compressed by 0.1 mm, respectively, at a rate of 0.005 mm/s. It was concluded based on modelling that any pedicle deformation would be small and it was ignored. Hysteresis loops were observed through loading and unloading cycles. For the relaxation test, the joints were elongated 0.2 mm in approximately 0.5 s at a rate of 0.4 mm/s to approximate a step function, and the relaxing stress was recorded until its rate of change was less than 0.1 % s^{-1}.

GEOMETRY

Figure 1b shows our 3D FE model of the ISJ. The model has six components: LPI, SH, joint capsule, two cartilage layers, and SF. The articular surfaces of the LPI and SH are approximately flat and their cross-sections can be approximated as elliptical, as done by Zhang and Gan (2011) and Jiang and Gan (2018), who measured the longest and shortest diameters for two sets of eight different ISJs each. Based on their measurements, we use $a_1 = 0.9$ mm for the longest diameter and $b_1 = 0.6$ mm for the shortest diameter. We assume that the SH has the same cross-sectional shape, aligned with and parallel to the LPI, and that the opposing surfaces are both planar (see figure 1c).

The articular cartilage layers completely cover the bones except for a very narrow gap (0.01 mm) next to the joint capsule. The sidewalls of the cartilage are inclined to avoid sharp corners and to avoid having contact with the capsule during deformation. This also approximates the rounded shapes of the

bony surfaces and the cartilage layers at the corners. The thickness is t_2 = 0.09 mm for both cartilage layers, decreasing to t_1 = 0.01 mm at the sides. The shortest and longest diameters of the cartilage-layer surfaces facing the SF are b_3 = 0.38 mm and a_3 = 0.57 mm, respectively.

The joint capsule is initially modelled as a straight elliptical tube, with a constant thickness t_c = 0.08 mm, connected to the exterior sides of the bones. The synovial gap is enclosed by the capsule, cartilage layers and bones, and is filled entirely with SF. Based on histological sections (e.g., figure 1a, and those published by Karmody et al., 2009), and on the appearance of the ISJ during experiments under a microscope (Feizollah et al., 2019), we assume that the real capsule has a curved profile when no force is applied to the joint. We create such a profile from the initial straight profile by compressing the joint axially while holding the geometry of the bones and cartilage layers fixed and treating the SF and the capsule as incompressible (figure 1d). The geometry of the joint with the curved profile of the capsule was then exported and used as the unloaded joint shape. The free length of the initial straight version of the capsule (i.e., the length of the part not attached to the bones) is L_c = 0.36 mm, and the final gap between the bony surfaces is h_b = 0.3 mm. The parameters L_c and h_b together determine the curved shape of the capsule in its neutral state. Although ranges of these two parameters were taken from histological sections, the actual values used were found by fitting the FE model to the experimental tension and compression data, as described below in the Material Properties section.

The simulations were run in FEBio 2.3.1, an open-source nonlinear FE solver suitable for biomechanics and biophysics applications (Maas et al. 2012). The geometry was developed and meshed in Preview 1.17.2, a preprocessor associated with FEBio. We used hexahedral solid elements to mesh all of the component geometries and connected them together by sharing all of the nodes at the boundary surfaces between neighbouring components. The final discretized geometry had 47556 nodes and 44800 elements. To check the adequacy of the resolution, we performed a mesh-convergence

analysis by increasing the number of nodes in all directions (azimuthal, radial, and longitudinal) by 50%, resulting in 149812 nodes and 143820 elements. The changes in the results were less than 7% in the tension and compression tests. Ideally, further mesh refinement would have been done, but construction of the model geometry was very time-consuming because, as explained above, we ran simulations for constructing the capsule and cartilage geometries, and then had to match these geometries and their meshes with the other components in order to manage their contacts at shared surfaces and to have a smooth mesh. The non-linear simulations themselves were time-consuming. Therefore, in view of the unavoidable uncertainties in the geometry and material properties, we decided to use 47556 nodes for all of the simulations in this paper, which resulted in sufficient numerical precision in the results and run times of 3 to 5 hours for each simulation. The simulations were run on the McGill University High Performance Computing facility (Guillimin cluster) which provides access to processors of type Dual Intel Sandy Bridge EP E5-2670 (8-core, 2.6 GHz, 20MB Cache, 115W) and Quad Intel Sandy Bridge EP E5-4620 (8-core, 2.2 GHz, 16MB Cache, 95W). We ran simulations on one node with 4 processors.

In our simulations the SH is fixed, and the LPI is displaced by specified amounts. The corresponding applied force is then calculated by integrating the normal stress over the LPI top surface. The SF always remains connected to the surrounding components.

CONSTITUTIVE EQUATIONS

Three different material models were used in this work to describe the components of the joint: linear elastic, Mooney-Rivlin, and Veronda-Westmann. Linear elasticity assumes linear relationships between the stress and strain tensor components, which is valid only for small deformations. Therefore, we used this model for the cartilage layers and the bones because they experience deformations that are small compared to their dimensions. An isotropic linear model is completely described with two parameters,

for example, Young's modulus E and the Poisson ratio v.

For large deformations it is common to use hyperelastic models where the nonlinear stress-strain relationship is derived from a strain-energy function. The strain-energy function for the Mooney-Rivlin (Mooney 1940) model is

$$W = C'(I_1 - 3) + C''(I_2 - 3) + W_{vol}(J), \tag{1}$$

where C' and C'' are material constants, $W_{\text{vol}}(J)$ is the volumetric energy, and

$$I_1 = \lambda_1^2 + \lambda_2^2 + \lambda_3^2, \quad I_2 = \lambda_1^{-2} + \lambda_2^{-2} + \lambda_3^{-2}, \tag{2}$$

where I_1 and I_2 are strain invariants and $\lambda_1, \lambda_2, \lambda_3$ are the stretches. $J = \lambda_1\lambda_2\lambda_3$ is the determinant of the deformation gradient tensor. For a constant-volume (incompressible) deformation, $J = 1$. If the volume of the material is decreased or increased by the deformation, then $J < 1$ or $J > 1$, respectively. The volumetric energy $W_{\text{vol}}(J)$ is the energy due to the changes of the material volume during deformation. For nearly incompressible materials, FEBio (Maas et al. 2012) defines this energy as

$$W_{\text{vol}} = \frac{1}{2}k[\log(J)]^2, \tag{3}$$

where k is the bulk modulus. As k increases, the energy required for the volume change increases, making the material less compressible. A special case of the Mooney-Rivlin model is the neo-Hookean model in which $C''=0$.

The model of Veronda and Westmann (1970) expresses the strain-energy function as

$$W = c_1[e^{\beta(I_1 - 3)} - 1] + c_2(I_2 - 3) + W_{\text{vol}}(J), \tag{4}$$

where β, c_1 and c_2 are material constants. FEBio uses a simplifying assumption, $c_2 = -c_1\beta / 2$ (Maas et

al. 2018), which reduces the number of parameters in equation 4, resulting in

$$W = C_1[e^{C_2(I_1-3)}-1]-\frac{C_1C_2}{2}(I_2-3)+W_{\text{vol}}(J), \tag{5}$$

where C_1 and C_2 are the material constants.

For modelling viscoelasticity, FEBio calculates the second Piola-Kirchhof stress tensor $\boldsymbol{S}(t)$ as the convolution of a normalized relaxation function $G(t)$ with the derivative of the elastic stress $\boldsymbol{S}^e$ (Maas et al. 2018):

$$\boldsymbol{S}(t)=\int_0^t G(t-u)\left(\frac{\mathrm{d}\boldsymbol{S}^e}{\mathrm{d}u}\right)\mathrm{d}u, \tag{6}$$

where t is time. Assuming that $\boldsymbol{S}^e$ is the long-term elastic response of the material, FEBio uses the following form of the Prony series for $G(t)$ (Maas et al. 2018):

$$G(t)=1+\sum_{i=1}^{N} g_i\exp(-t/\tau_i), \tag{7}$$

where τ_i are the time constants, g_i are the relaxation coefficients, and N is the number of terms in the Prony series.

MATERIAL PROPERTIES

We have been unable to find any publications on direct measurement of the mechanical properties of the various components of the ISJ. We therefore used material properties from other synovial joints in the human body, as explained below.

Cartilage layers: The elastic and viscoelastic properties (i.e., disregarding time effects and including time effects, respectively) of cartilage have been measured for cartilages taken from different parts of

the body, particularly the knee joints (e.g., Hayes and Mockros, 1971 for the human knee, June et al., 2006 for the bovine knee, and Kumar et al., 2018 for the osteoarthritic human knee). For the elastic part (i.e., the $\boldsymbol{S}^{\mathrm{e}}$ part of equation 6), we use an isotropic linear-elastic material with the same Young's modulus and Poisson ratio as were used by Funnell et al. (2005), E_{c}=10 MPa (after Bader and Lee 2000) and $\nu_{\mathrm{c}} = 0.3$. Cartilage shows significant stress relaxation under constant strain because of its multiphasic nature (e.g., June et al., 2006; Smyth, 2013). Here, for the $G(\cdot)$ part of equation 6, we use a two-term Prony series to model cartilage with time constants $\tau_{1,\mathrm{c}} = 1.5$ s and $\tau_{2,\mathrm{c}} = 35$ s; and coefficients $g_{1,\mathrm{c}} = 0.8$ and $g_{2,\mathrm{c}} = 0.5$. We found these values by fitting equation 7 to experimental stress relaxation results (Smyth and Green 2015) for equine articular cartilage, which is believed to be similar to human cartilage (Malda et al. 2012).

Joint capsule: The joint capsule experienced quite large deformations under the mechanical tests by Zhang and Gan, and therefore cannot be modelled as a linear-elastic material. Measurements of capsule mechanical properties have shown significant differences when comparing capsules from different joints of the body or different parts of the same joint capsule (e.g., Kaltsas, 1983; Hewitt et al., 2002). Rainis et al. (2009) and Browe et al. (2014) successfully modelled the mechanical behaviour of the shoulder-joint capsule using the Veronda-Westmann strain-energy function. We initially tried to use the material properties of the shoulder joint for modelling the ISJ capsule (Soleimani et al. 2018), but concluded that the ISJ capsule must be much softer than the shoulder capsule.

We calculated the capsule geometry and elastic properties by fitting our model to the experimental results of Zhang and Gan (2011), reproduced here in figure 2. The parameters to be fitted were L_{c} and h_{b} (see figure 1b); the capsule elastic constants; and the position of the experimental zero along the displacement axis, as discussed at the beginning of the Results section. We used the Veronda-Westmann strain-energy function and adjusted the values for C_1 and C_2 in equation 5 to fit our FE model to the

results of the experimental tension and compression tests. Based on our previous observations (Soleimani et al. 2018), we took initial values of C_1 and C_2 that were smaller by a factor of 10 than the shoulder-joint-capsule constants that we calculated in that study, resulting in C_1 = 6.5 kPa and C_2 =1. We changed each of these parameters to understand how they affect the results of the FE simulations, and then iteratively adjusted them manually in order to reduce the error between the FE model and the experimental data. The initial values of L_c and h_b were 0.33 mm and 0.3 mm, respectively, roughly estimated from various histological sections. The bulk modulus was fixed at k=1 GPa.

In the final fitted model the material parameters were C_1 = 70 kPa and C_2 =1.8, with C_1 actually being similar to the value in Soleimani et al. (2018) but C_2 much smaller. Considering equation 5, this suggests that the ISJ capsule shows less non-linearity than the shoulder joint capsule does, although their behaviour maybe quite similar at small displacements. The geometrical parameters were L_c = 0.36 mm and h_b = 0.3 mm as mentioned above in the section on Geometry.

Various models have been used to describe experimental stress relaxation results for different joint capsules (Funk et al., 1999; Bonifasi-Lista et al., 2005; Dommelen et al., 2005, 2006; Davis, 2013; Criscenti et al., 2015). We used a two-term Prony series to model the viscoelastic effects of the capsule with time constants $\tau_{1,cp}$= 5 s and $\tau_{2,cp}$= 100 s and coefficients $g_{1,cp}$ = 0.9, $g_{2,cp}$ = 0.1. These parameter values fit within the range of those determined by Dommelen et al. (2006), Davis (2013) and Criscenti et al. (2015).

Synovial fluid: Here we used viscoelastic solid elements to model the SF confined within the synovial gap. We tried to mimic the liquid behaviour by using a very soft neo-Hookean material that was made highly viscous by assigning small time constants and large coefficients for the Prony series. We assumed that the energy dissipation mostly occurs in the SF because of its high viscosity and its large deformations. Therefore, we tried to keep the SF relaxation coefficients larger than those of the other

components. However, there is a convergence problem for very small elastic constants combined with very high relaxation coefficients, particularly during the fast elongation of the relaxation test. As a compromise, we fixed the SF elastic constant C_{sf} = 10 kPa, and used a three-term Prony series with time constants $\tau_{1,sf}$= 0.01 s, $\tau_{2,sf}$= 0.1 s and $\tau_{3,sf}$= 1 s with relaxation coefficients $g_{1,sf}$ = 1, $g_{2,sf}$ = 0.4, $g_{3,sf}$ = 0.3. The bulk modulus was fixed at k=1 GPa.

Bone: The LPI and the SH were modelled as an isotropic linear-elastic material. The Young's modulus of bone varies for different bones in the body, for different parts of the same bone, and even for different directions in the same bone. Values in the literature fall in the range from 1 to 27 GPa (Funnell et al. 2005). Following Zhang and Gan (2011), we used E_b = 14.1 GPa for Young's modulus and ν_b = 0.3 for the Poisson ratio. This value of E_b is within the range of 16 ± 3 GPa that Soons et al. (2010) measured for rabbit middle-ear ossicles. Because the soft tissue in the joint is several orders of magnitude more flexible than the bone, the joint mechanical behaviour is expected to have low sensitivity to this uncertainty in the bone Young's modulus. We assume that damping in the bones is negligible.

Mass density: The density of the soft tissue (capsule, cartilage, and SF) is taken to be 1000 kg/m^3, which is almost the same as the value estimated by Funnell and Laszlo (1982). The bone density is taken to be 2000 kg/m^3 which is within the range discussed by Maftoon et al. (2015).

Results

TENSION, COMPRESSION, AND STRESS-RELAXATION TESTS

An important aspect of the experimental results of Zhang and Gan (2011) is the very soft mechanical behaviour of the joint close to the zero force, particularly during tension. This, together with possible effects related to preconditioning, may cause an incorrect estimation of the zero-force configuration in

the experiments. Here, while adjusting the four parameters stated above (L_c, h_b, C_1, C_2), we also shifted the experimental zero along the displacement axis to improve the fit between our FE model and the experiment.

Figure 2a shows the fit between our FE model results and the experimental tension and compression results. In this figure, we have moved the experimental data 0.02 mm toward negative displacements. Note that we need a very small amount of force (less than 0.01 N) to have this displacement, and Zhang and Gan (2011) already applied 0.001 N of preload on the specimen as the initial state. This 0.02-mm shift is applied in all of our tension and compression results, including the hysteresis loops. The FE model and experimental data agree well except around the zero-force point, where we were unable to reduce the maximum discrepancy of 0.02 N at a displacement of −0.02 mm.

To fit the experimental relaxation results, we used fixed time constants for the Prony series (see above) and then calculated the coefficients by fitting the model to the relaxation measurements. The final result is shown in figure 2b. The difference between the fully relaxed state of the FE model and that of the experimental mean is about 60% of the standard deviation of the experimental results.

After finding the material and geometrical properties of the capsule and SF using the tension, compression and relaxation tests, we simulated a hysteresis test with our FE model and compared the results with the experimental data. Figure 3 shows this comparison. (We did not model the two-minute waiting time between the tension and compression tests that was implemented by Zhang and Gan (2011) in their experiments.) The disagreement in the loading curves is at least partly because the experimental results in figure 2, to which the model was fitted, are the averages of the measurements on several specimens, while here we are comparing our model with the results of only one of the specimens, because it was the only specimen for which both loading and unloading curves were given. (We could not refit the model to this one specimen because its individual relaxation results were not

given.) Our model predicts a hysteresis behaviour that is comparable to the experimental data of the ISJ, showing a larger area within the hysteresis loop in compression than in tension. The hysteresis loop in tension has an area of 0.0041 Nmm in the FE model and almost 0.0036 Nmm in the experimental data. In compression, the loop has an area of 0.0082 Nmm in the FE model and about 0.0069 Nmm in the experimental data.

SENSITIVITY ANALYSIS

As explained in the Methods section, the lack of data introduces large uncertainties in the ISJ material and geometrical properties. Here we performed a sensitivity analysis on our ISJ model to understand how each parameter affects the mechanical response of the model. We changed each parameter by ±10% and simulated the tension and compression tests. We changed the curved shape of the capsule by changing the capsule length L_c by ±10% while maintaining a constant gap h_b between the bony surfaces. Different parameters have different levels of uncertainty, and that uncertainty is often much greater than ±10%, but using ±10% uniformly allows a comparison of the relative effects of the parameters, at least for small changes, without too much interaction among the effects.

Figures 4a and 4b show the force-displacement curves for changes in the geometrical parameters (i.e., cartilage thickness and capsule length) while figures 4c to 4e show the curves for changes in material properties (i.e., capsule elastic constants C_1 and C_2 and cartilage Young's modulus). The capsule length and the cartilage thickness can be seen to have larger effects on the mechanical behaviour of the ISJ than the material properties do.

The effect of making the capsule more or less curved is almost entirely for tension and not for compression, while the opposite is true for the cartilage thickness. Making the capsule more curved increases asymmetry but decreases non-linearity, while an increase in cartilage thickness increases both asymmetry and non-linearity.

Similar observations apply for the material properties of the capsule and the cartilage. The cartilage Young's modulus E_c affects the compression curve almost exclusively, such that increasing E_c increases the asymmetry and the non-linearity. The elastic constants of the capsule have larger effects in tension than in compression, such that increasing either C_1 or C_2 decreases the asymmetry but increases the non-linearity. The most influential material property is C_2; in equation 5, C_2 is in the exponent and can strongly influence the non-linearity in the model, while C_1 should have more influence on the stiffness of the material and less on its non-linearity.

We produced plots like those in figure 4 for other material properties including the bone Young's modulus and Poisson ratio, the capsule compressibility, the SF elastic constant and compressibility, and the cartilage Poisson ratio. These other parameters all had negligible effects that were hardly or not at all visible in such plots. Changes of ±10% in the bulk moduli k_{cp} and k_{sf}, for the capsule and the SF, respectively, have practically no effect on the behaviour (less than 0.03% at the maximum loads) because we made them large enough to make the capsule and the SF incompressible. The same thing is true for the Young's modulus E_b for the bone (less than 0.02% difference at the maximum loads), because it is large enough that it makes the bones behave like rigid bodies compared to the soft tissue. Increasing or decreasing the Poisson ratios ν_b and ν_c, which are related to the compressibility (±10% changes in ν_b and ν_c corresponded to an 18% increase and a 13.5% decrease, respectively, in the bulk moduli of the bone and cartilage) causes only small changes in the behaviour (less than 4% at the maximum loads). The elastic constant C_{sf} of the SF has only a minor effect on the behaviour (less than 3% at the maximum loads) because we chose the SF material properties to be very flexible compared to the other materials.

Discussion

It is extremely difficult to include all of the details of an ISJ in a FE model, so we have to simplify the

geometry with plausible assumptions. Here we assumed that the LPI and SH have the same flat cross section and are parallel and aligned with each other. However, it is clear from our histological sections and those shown by Karmody et al. (2009) that the LPI actually has a somewhat convex articulating surface while the SH is concave, and they are not necessarily aligned or parallel, at least not after histological processing. We also assumed that the cartilage layers have the same thickness on both articulating surfaces while Karmody et al. (2009) concluded that the cartilage on the LPI is 3 to 4 times thicker than that of the SH. We have also neglected the presence of calcified cartilage between the uncalcified cartilage layers and the bones. These assumptions were also used in all previous ISJ models. Karmody et al. observed a dense fibrous meniscus within the synovial gap, but we have not modelled it because, first, it was not observed in our histological sections, and second, its material properties, shape, and links to the other components are not clear.

Biological tissue characteristics typically vary a lot from sample to sample, which causes considerable uncertainty when constructing an ISJ model. The dimensions and shape of each component obtained from histological sections (e.g., figure 1a) or from X-ray microCT scans of post-mortem temporal bones may differ from the in-vivo joint configuration because of, for example, dehydration of the soft tissue, dislocation of the bones, or processing of the specimen. For example, the amount of SF within the synovial gap, the thickness of the synovial gap, and the curved shape of the capsule when no force is applied to the joint cannot be reliably determined. It is even unclear whether the joint is under stress when no pressure is applied to the tympanic membrane. Another challenge is to determine the free length of the capsule, as it is not obvious where and how the capsule is connected to the lenticular process. Karmody et al. (2009) concluded that the joint capsule covers the full height of the lenticular process, but the beginning of a bonding between them is not obvious.

We previously showed that the curved shape of the capsule and the amount of SF within the synovial

gap can produce asymmetry between tension and compression tests (Soleimani and Funnell, 2018; Soleimani et al., 2018). In our present model, we used the curved shape of the capsule (controlled by the length parameter L_c and the gap parameter h_b) to produce asymmetry, and used both the capsule shape and the capsule material properties to match the behaviour that is observed experimentally. Together with a shift of the experimental zero, we thus adjusted 5 parameters (L_c, h_b, C_1, C_2, and the shift of the experimental zero) to fit our FE model to the experimental data. We cannot be sure that a good match could not be obtained with other combinations of these parameters. In particular, a well-designed automatic fitting algorithm might result in even better matching than our manual trial-and-error method did. However, the complications related to the geometry development would make an automatic approach difficult to implement for this model.

The largest difference between the FE model and the experimental data in the tension and compression tests (figure 2a) is at −0.02 mm, exactly where we applied the shift of the experimental zero. The difference is larger than the standard deviation of the experimental data for deformations between −0.05 mm and 0.02 mm. We were unable to make a good match in this region. It might be possible to produce a good match by using a different hyperelastic model with a differently shaped non-linearity, or by implementing contact between the cartilage layers in compression.

For the stress relaxation tests, the experimental step function was applied over an interval of 0.5 s, which is small enough when compared to the time constants used in the model for the capsule or cartilage, but quite large when compared to the time constants used for the SF. We used the same speed for the step function in our FE simulations. This means that the SF is already partially relaxed at the end of the step function, and the observed stress relaxation is actually less than the real relaxation of the joint. (We need to use short time constants for the SF to model its liquid-like behaviour.) The speed of the step function may not be fast enough for the SF in the experimental data either.

The rheological properties of SF are normally described by the viscosity and the dynamic moduli as functions of shear rate or frequency (e.g., Fam et al., 2007). It is possible in principle to obtain the time constants and the relaxation coefficients by fitting the Fourier transform of the Prony series to experimentally measured complex moduli. However, the correct capturing of small time constants requires data over a wide range of frequencies, which are unavailable because of the limitations of mechanical rheometry.

It is clear that the relaxation behaviour of the joint is a function of the combination of the relaxation behaviours of each component. The cartilage layers experience less deformation in this model than the capsule and the SF do, and therefore the relaxation of the cartilage was found to have relatively little impact on the relaxation of the joint. We chose the time constants and the relaxation coefficients of the cartilage and the capsule based on available experimental data, as stated in the Methods section. Because the viscoelastic properties of the SF are usually measured by means of the dynamic moduli, we were unable to find any direct experimental data for the relaxation behaviour of the SF. However, we expect almost complete relaxation for the SF because of its liquid-like behaviour. We tried using three short time constants and high relaxation coefficients for the SF, but we were unable to model the nearly complete relaxation of the SF because very high relaxation coefficients prevented convergence of the FE simulation. This approximate SF model might suffice for quasi-static or low-frequency loads but more realistic models might be necessary for high-frequency loads. The FE models of Jiang and Gan (2018) suggested that SF viscosity affects the ISJ mechanical behaviour more at higher frequencies.

The FE model could fairly successfully predict the nature of the hysteresis loops in tension and compression tests (figure 3), providing further validation for the FE model. The hysteresis loop is larger in compression than in tension, showing that more energy is dissipated in compression. The better

model fit in compression may be because this particular specimen has a mechanical behaviour that is close to the experimental average in compression but a little different from the average in tension.

Although computational fluid dynamics (CFD) has recently been implemented using FEBio (Ateshian et al. 2018), the current version of FEBio itself does not support CFD or fluid-solid interactions yet. This was the reason for using solid elements to model the SF. An interesting extension to this work would be to use true liquid elements to model the SF.

The simplified applied loads and boundary conditions presented in this paper clearly cannot describe what happens in the intact middle ear and how the lenticular-process and stapes-head motions are related under physiological stimuli of different frequencies and levels. . More realistic loads and boundary conditions can be obtained by embedding ISJ models in complete middle-ear models (e.g., Funnell et al.; 2005; Gan & Wang, 2015; Qian & Funnell, 2019). Such models can then be compared with behaviour measured in situ (e.g., Huttenbrink, 1988; Gea, 2010; Jiang & Gan, 2018; Feizollah et al., 2019).

Conclusions

This FE model of the ISJ gives a good fit to the experimental data of tension, compression, and stress relaxation tests. We did not use different assumptions for the tension and compression tests to model their strong asymmetry. The sensitivity analysis suggests that the asymmetry comes mainly from the geometry of the joint capsule and the thickness of the cartilage. The sensitivity analysis showed that ±10% changes of the geometrical parameters affect the joint mechanical behaviour more than ±10% changes in the material properties do. (The capsule geometrical and material properties tend to affect mostly the tension curve while the cartilage properties affect mostly the compression curve.) Among

the material properties, the capsule elastic constants and the cartilage Young's modulus have the largest effects. Therefore, particular attention should be given to the geometrical and material properties of the articular cartilage layers and the joint capsule in future work. It will be important to obtain better observations of the geometry of the ISJ under natural unloaded conditions.

This model was deposited in BioModels (Chelliah et al. 2015) and assigned the temporary submission identifier MODEL1905070001.

Acknowledgements

This work was supported by the Canadian Institutes of Health Research and the Natural Sciences and Engineering Research Council of Canada. The authors thank Calcul Québec and Compute Canada for providing high performance computation facilities for this research. The authors also thank Clarinda C. Northrop for providing us with valuable histological images.

Conflict-of-interest disclosure statement

The authors declare that they have no conflict of interest.

References

Ateshian GA, Shim JJ, Maas SA, Weiss JA (2018) Finite element framework for computational fluid dynamics in FEBio. J Biomech Eng 140:021001-021001–17. doi: 10.1115/1.4038716

Bader D, Lee D (2000) Structure – properties of soft tissues articular cartilage. In: Pergamon Materials Series. Elsevier, pp 75–103

Bonifasi-Lista C, Lake SP, Small MS, Weiss JA (2005) Viscoelastic properties of the human medial collateral ligament under longitudinal, transverse and shear loading. J Orthop Res Off Publ Orthop Res Soc 23:67–76. doi: 10.1016/j.orthres.2004.06.002

Browe DP, Voycheck CA, McMahon PJ, Debski RE (2014) Changes to the mechanical properties of the glenohumeral capsule during anterior dislocation. J Biomech 47:464–469. doi: 10.1016/j.jbiomech.2013.10.040

Chelliah V, Juty N, Ajmera I, et al (2015) BioModels: ten-year anniversary. Nucleic Acids Res 43:D542–D548. doi: 10.1093/nar/gku1181

Criscenti G, De Maria C, Sebastiani E, et al (2015) Quasi-linear viscoelastic properties of the human medial patello-femoral ligament. J Biomech 48:4297–4302. doi: 10.1016/j.jbiomech.2015.10.042

Davis FM (2013) Nonlinear viscoelastic behaviour of ligaments and tendons: models and experiments. Ph.D. thesis, Virginia Polytechnic Institute and State University

Decraemer WF, Maas SA, Funnell WRJ (2015) Finite-element modelling of the synovial fluid and contact in the incudostapedial joint. In: 7th International Symposium on Middle-Ear Mechanics in Research and Otology. Aalborg, Denmark

Dommelen JAW van, Jolandan MM, Ivarsson BJ, et al (2005) Pedestrian injuries: viscoelastic properties of human knee ligaments at high loading rates. Traffic Inj Prev 6:278–287. doi: 10.1080/15389580590969436

Dommelen JAW van, Jolandan MM, Ivarsson BJ, et al (2006) Nonlinear viscoelastic behavior of human knee ligaments subjected to complex loading histories. Ann Biomed Eng 34:1008–1018. doi: 10.1007/s10439-006-9100-1

Fam H, Bryant JT, Kontopoulou M (2007) Rheological properties of synovial fluids. Biorheology 44:59–74

Feizollah S, Soleimani M, Funnell WRJ (2019) Imaging of the gerbil incudostapedial joint. In: Association For Research In Otolaryngology (ARO) 42nd Annual Winter Meeting. Baltimore, MD, USA

Funk JR, Hall GW, Crandall JR, Pilkey WD (1999) Linear and quasi-linear viscoelastic characterization of ankle ligaments. J Biomech Eng 122:15–22. doi: 10.1115/1.429623

Funnell WR, Laszlo CA (1982) A critical review of experimental observations on ear-drum structure and function. ORL J Otorhinolaryngol Relat Spec 44:181–205. doi: 10.1159/000275593

Funnell WRJ, Daniel SJ, Alsabah B, Liu H (2006) On the coupling between the incus and the stapes. In: Auditory Mechanisms: Processes and Models. World Scientific, pp 115–116

Funnell WRJ, Heng Siah T, McKee MD, et al (2005) On the coupling between the incus and the stapes in the cat. J Assoc Res Otolaryngol 6:9–18. doi: 10.1007/s10162-004-5016-3

Gan RZ, Wang X (2015) Modeling microstructure of incudostapedial joint and the effect on cochlear

input. AIP Conf Proc 1703:060011. doi: 10.1063/1.4939366

Gea S (2010) The application of microtomography in research of middle ear mechanics of gerbil and human at static pressure changes. Ph.D. thesis, University of Antwerp

Ghosh SS, Funnell WRJ (1995) On the effects of incudostapedial joint flexibility in a finite-element model of the cat middle ear. In: IEEE EMBS 17th Annual Conference

Gottlieb PK, Vaisbuch Y, Puria S (2018) Human ossicular-joint flexibility transforms the peak amplitude and width of impulsive acoustic stimuli. J Acoust Soc Am 143:3418. doi: 10.1121/1.5039845

Hayes WC, Mockros LF (1971) Viscoelastic properties of human articular cartilage. J Appl Physiol 31:562–568. doi: 10.1152/jappl.1971.31.4.562

Hewitt JD, Glisson RR, Guilak F, Vail TP (2002) The mechanical properties of the human hip capsule ligaments. J Arthroplasty 17:82–89

Jiang S, Gan RZ (2018) Dynamic properties of human incudostapedial joint—Experimental measurement and finite element modeling. Med Eng Phys 54:14–21. doi: 10.1016/j.medengphy.2018.02.006

June RK, Barone JR, Fyhrie DP (2006) Cartilage stress-relaxation described by polymer dynamics. In: Annual Meeting of the Orthopaedic Research Society

Kaltsas DS (1983) Comparative study of the properties of the shoulder joint capsule with those of other joint capsules. Clin Orthop 20–26

Karmody CS, Northrop CC, Levine SR (2009) The incudostapedial articulation: new concepts. Otol

Neurotol 30:990–997. doi: 10.1097/MAO.0b013e3181b0fff7

Kumar R, Pierce DM, Isaksen V, et al (2018) Comparison of compressive stress-relaxation behavior in osteoarthritic (ICRS graded) human articular cartilage. Int J Mol Sci 19:413. doi: 10.3390/ijms19020413

Maas SA, Ellis BJ, Ateshian GA, Weiss JA (2012) FEBio: finite elements for biomechanics. J Biomech Eng 134:011005. doi: 10.1115/1.4005694

Maas SA, Rawlins D, Weiss JA, Ateshian GA (2018) FEBio user's manual version 2.8.

Maftoon N, Funnell WRJ, Daniel SJ, Decraemer WF (2015) Finite-element modelling of the response of the gerbil middle ear to sound. JARO J Assoc Res Otolaryngol 16:547–567. doi: 10.1007/s10162-015-0531-y

Malda J, Benders KEM, Klein TJ, et al (2012) Comparative study of depth-dependent characteristics of equine and human osteochondral tissue from the medial and lateral femoral condyles. Osteoarthritis Cartilage 20:1147–1151. doi: 10.1016/j.joca.2012.06.005

Mooney M (1940) A Theory of Large Elastic Deformation. J Appl Phys 11:582–592. doi: 10.1063/1.1712836

O'Connor KN, Cai H, Puria S (2017) The effects of varying tympanic-membrane material properties on human middle-ear sound transmission in a three-dimensional finite-element model. J Acoust Soc Am 142:2836–2853. doi: 10.1121/1.5008741

Qi L, Funnell WRJ, Daniel SJ (2008) A nonlinear finite-element model of the newborn middle ear. J Acoust Soc Am 124:337–347. doi: 10.1121/1.2920956

Qian D, Funnell WRJ (2019) Finite-element modelling of middle-ear vibrations under pressurization. In: Association For Research In Otolaryngology (ARO) 42nd Annual Winter Meeting. Baltimore, MD, USA

Rainis EJ, Maas SA, Henninger HB, et al (2009) Material properties of the axillary pouch of the glenohumeral capsule: is isotropic material symmetry appropriate? J Biomech Eng 131:031007. doi: 10.1115/1.3005169

Smyth PA (2013) Viscoelastic behavior of articular cartilage in unconfined compression. Thesis, Georgia Institute of Technology

Smyth PA, Green I (2015) Fractional calculus model of articular cartilage based on experimental stress-relaxation. Mech Time-Depend Mater 19:209–228. doi: 10.1007/s11043-015-9260-1

Soleimani M, Funnell WRJ (2016) Deformation and stability of short cylindrical membranes. Int J Mech Sci 119:266–272. doi: 10.1016/j.ijmecsci.2016.10.017

Soleimani M, Funnell WRJ (2018) Mechanical behaviour of short membranous liquid-filled cylinders under axial loadings. Int J Mech Sci 145:138–144. doi: 10.1016/j.ijmecsci.2018.06.034

Soleimani M, Funnell WRJ, Decraemer WF (2018) A new finite-element model of the incudostapedial joint. AIP Conf Proc 1965:110003. doi: 10.1063/1.5038503

Veronda DR, Westmann RA (1970) Mechanical characterization of skin—Finite deformations. J Biomech 3:111–124. doi: 10.1016/0021-9290(70)90055-2

Zhang X, Gan RZ (2011) Experimental measurement and modeling analysis on mechanical properties of incudostapedial joint. Biomech Model Mechanobiol 10:713–726. doi: 10.1007/s10237-010-

0268-9

Figure captions

Fig. 1: A Histological section of human incudostapedial joint (Courtesy C. Northrop, Temporal Bone Foundation). **B** Cross-section of the FE model showing various components and geometrical variables. **C** A 3D view of the bisected FE model showing the mesh. **D** Schematic of the procedure of curving the capsule using FE simulations: on left is initial model, on right is exported model after some compression to curve the capsule with fixed cartilage geometry and fixed volume of the capsule and SF.

Fig. 2 The fit between the FE model and the experimental data. **A** Results for the tension and compression tests; the capsule material properties and its geometry are determined by this fitting. The experimental zero is moved to −0.02 mm. **B** Results for the relaxation test; the relaxation coefficients of the SF and the joint capsule are determined by this fitting.

Fig. 3 Comparison of the hysteresis loops between FE model and experimental data. Loading curves are indicated by solid arrows while unloading curves are indicated by dashed arrows. The area of the compression part of the hysteresis loop is almost twice the area for the tension part of the loop in both the experimental and FE cases.

Fig. 4 Effects of geometrical parameters and material properties on the tension and compression curves. Each parameter was changed by ±10%. A: Capsule curved shape (as determined by length L_c). B: Cartilage thickness, t_2. C & D: Capsule elastic constants C_1 & C_2, respectively. E: Cartilage Young's modulus, E_c. Capsule properties affect the tension curve more while cartilage properties affect the compression curve more.

Figure 1

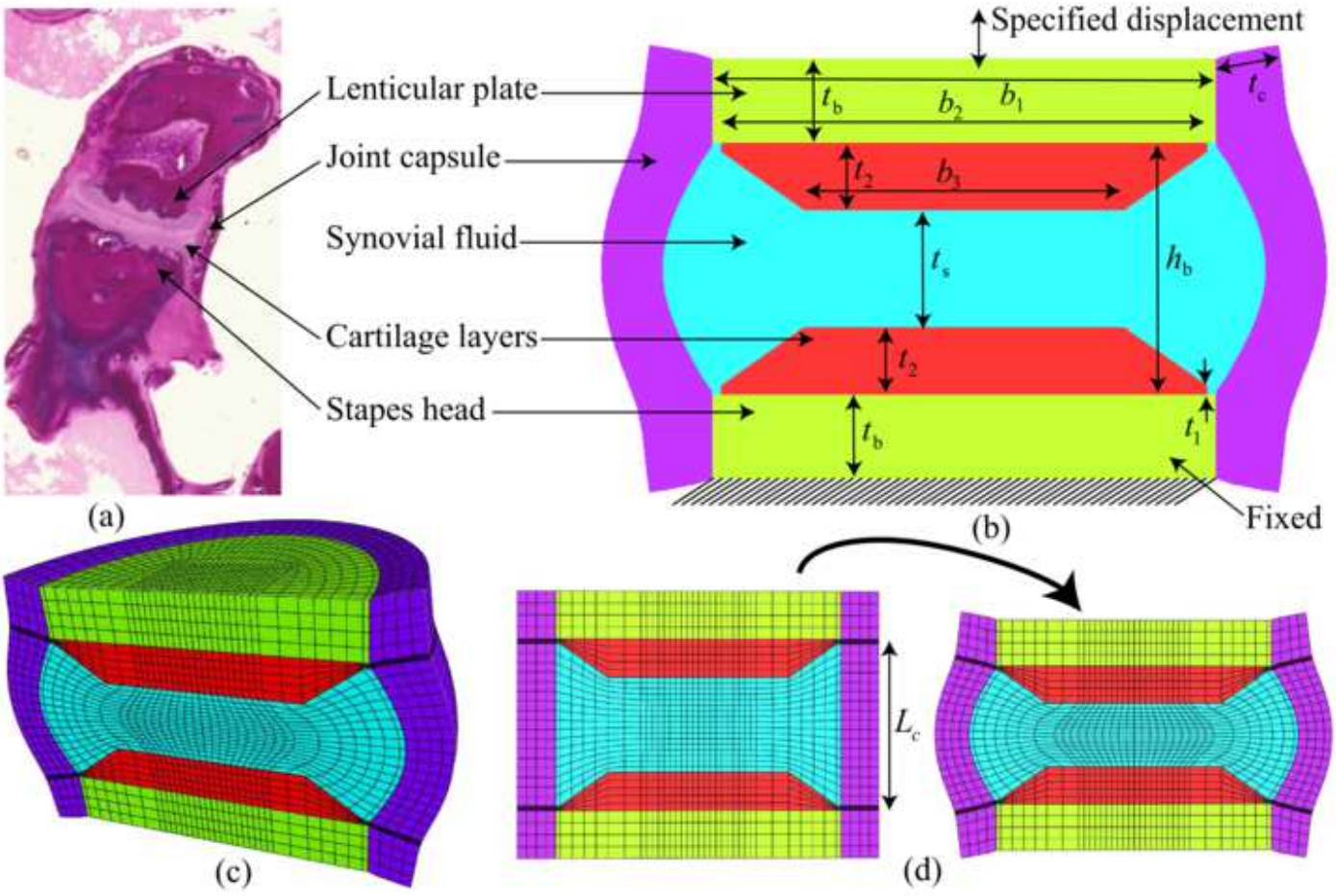
Lenticular plate
Joint capsule
Synovial fluid
Cartilage layers
Stapes head
(a)
Specified displacement
t_b
b_2
b_1
t_c
t_2
b_3
t_s
h_b
t_2
t_b
t_1
Fixed
(b)
(c)
L_c
(d)

Figure 2

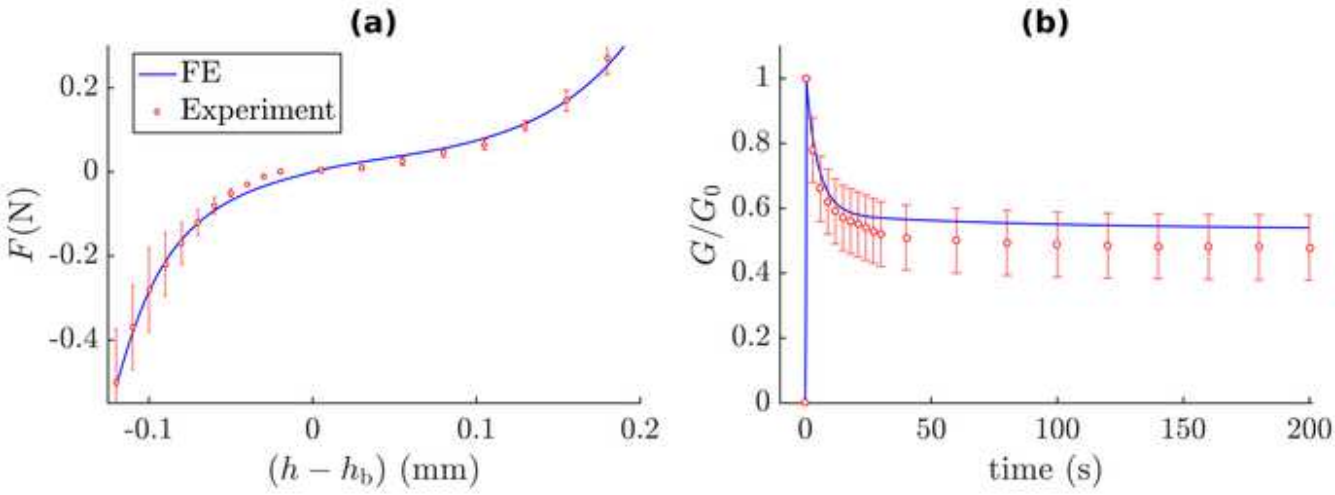
(a)
FE
Experiment
0.2
0
-0.2
-0.4
F(N)
-0.1
0
0.1
0.2
(h − h_b) (mm)
(b)
1
0.8
0.6
0.4
0.2
0
G/G_0
0
50
100
150
200
time (s)

Figure 3

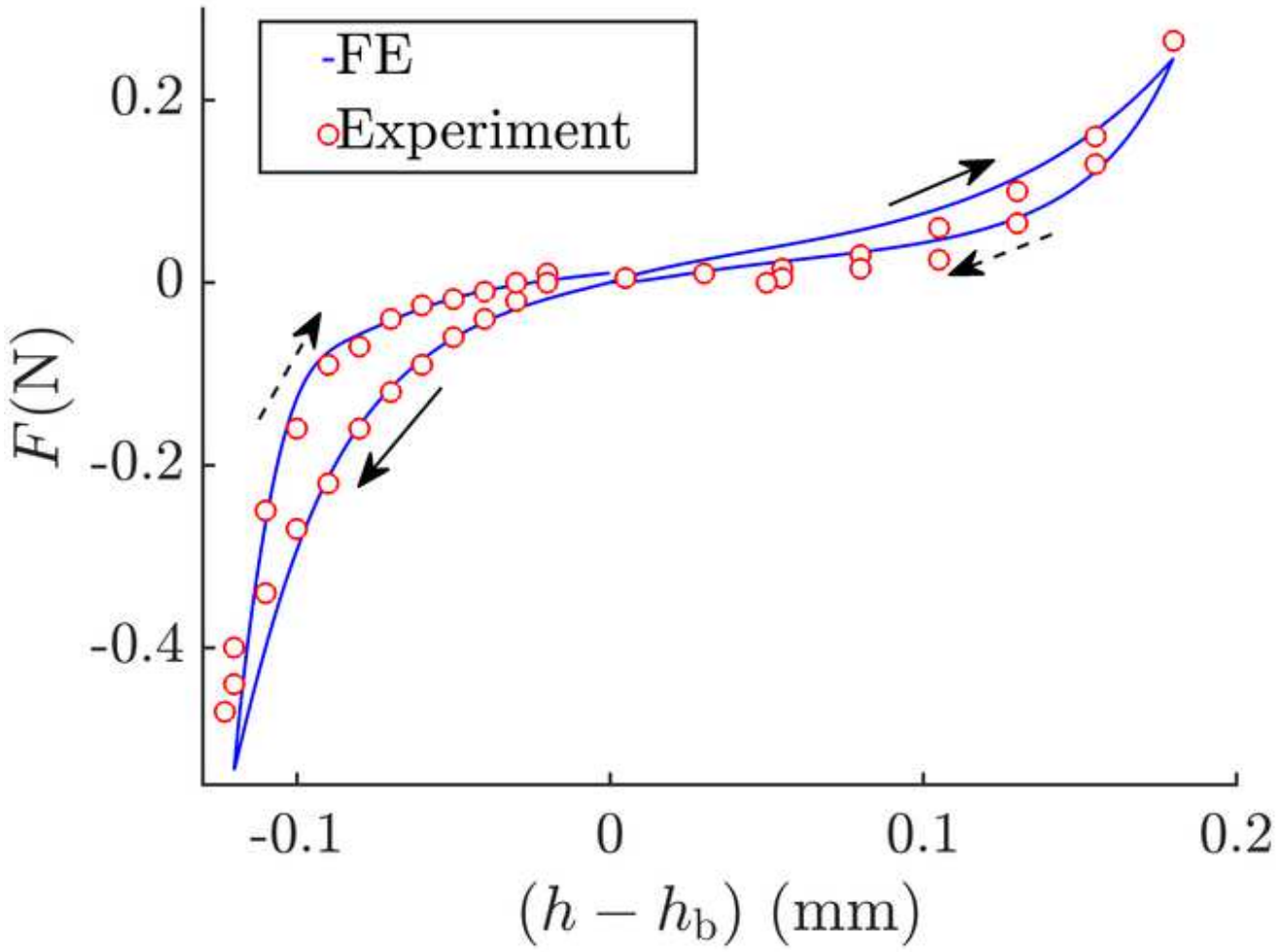

Figure 4